Int. J. Multiphase Flow Vol. 12, No. 6, pp. 861–889, 1986
Printed in Great Britain

0301-9322/86 $3.00 + 0.00
Pergamon Journals/Elsevier

A TWO-PHASE MIXTURE THEORY FOR THE DEFLAGRATION-TO-DETONATION TRANSITION (DDT) IN REACTIVE GRANULAR MATERIALS

M. R. BAER and J. W. NUNZIATO
Fluid and Thermal Sciences Department, Sandia National Laboratories, Albuquerque, NM 87185, U.S.A.

(*Received* 10 *September* 1985; *in revised form* 23 *February* 1986)

Abstract—In this paper, a two-phase mixture theory is presented which describes the deflagration-to-detonation transition (DDT) in reactive granular materials. The theory is based on the continuum theory of mixtures formulated to include the compressibility of all phases and the compaction behavior of the granular material. By requiring the model to satisfy an entropy inequality, specific expressions for the exchange of mass, momentum and energy are proposed which are consistent with known empirical models. The model is applied to describe the combustion processes associated with DDT in a pressed column of HMX. Numerical results, using the method-of-lines, are obtained for a representative column of length 10 cm packed to a 70% density with an average grain size of 100 μm. The results are found to predict the transition to detonation in run distances commensurate with experimental observations. Additional calculations have been carried out to demonstrate the effect of particle size and porosity and to study bed compaction by varying the compaction viscosity of the granular explosive.

1. INTRODUCTION

The modes of flame spread and the transition from deflagration to detonation (DDT) in gas-permeable, reactive granular materials have been the subject of extensive research—yet much remains to be understood. Generally, the process begins with ignition of a few grains by some external energy source. Initially, the combustion process is slow and dominated by heat conduction within and between grains. Andreev (1944) first postulated that the hot product gases generated during the early stage can penetrate into the pores of the unreacted material and, by preheating the grains, augment flame spread by several orders of magnitude above the deflagration rate driven by thermal conduction alone. This mode of flame spread can be self-accelerating and under conditions of strong confinement produce considerable gas pressures, which in turn leads to conditions favorable for detonation. This process is shown schematically in figure 1.

Experimental studies of this phenomena have been most useful in clarifying the physical processes during DDT. The pioneering work of Griffiths & Groocock (1960) confirmed the existence of a convectively-driven flame front during flame spread in a column of HMX and showed that the onset of detonation was well-removed from the location at which

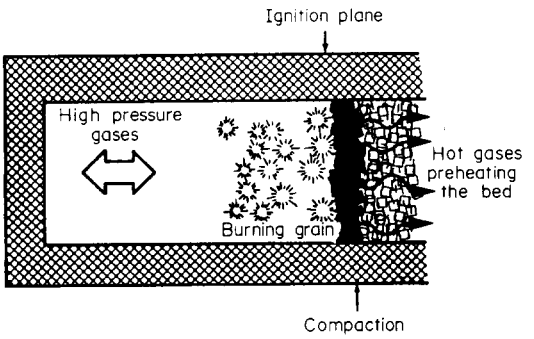

Figure 1. A schematic of flame spread in a heavily-confined column of explosive.

combustion began. Furthermore, this predetonation column length was shown to depend on the permeability of the granular bed. In similar studies, Price & Bernecker (1978) and Sandusky (1983) have studied the effects of high-pressure gas generation on mechanical load transfer to the solid granular material. Their studies have shown that considerable bed compaction occurs in the region ahead of the flame front. This, in turn, reduces the permeability of the granular bed and causes significant pressure buildup behind the flame front. This pressure further compresses the bed and accelerates the flame front. From these observations, it is evident that there is an important coupling of the thermal and mechanical processes associated with combustion, and that the mechanical processes are key factors in the formation of the shock wave and in achieving detonation. Once a shock wave is formed, local "hot spots" release additional energy which enhances wave growth to detonation. Plausible mechanisms for this localized heating are microscale shock focusing during pore collapse, plastic work heating and intergranular friction at grain boundaries or in regions of high shear; see, for example, Nunziato (1984).

In view of these general experimental conclusions, the process of DDT in a column essentially consists of four regimes: conductive burning, convective burning, compressive burning and detonation. As a result of rapid gas pressurization, detonation occurs when pressure disturbances in the combustion regions focus and reinforce each other. It is important to note that hot gas convection is not the only possible driving mechanism for DDT. In recent experiments, Campbell (1980) used a column of HMX imbedded with gas-"impermeable" diaphragms and demonstrated that predetonation lengths were essentially the same as those found for columns without the diaphragms. This suggests that one important DDT process is the mechanical load transfer from the gas to the solid phase.† This load transfer can occur either through the use of plugs in the flow such as diaphragms or by the drag forces acting on the grains during convective flow which cause compaction and the formation of a plug.

It is clear that the coupled thermal–mechanical processes associated with the combustion of a granular explosive must be included in any complete model of the flow field. However, the formulation of the conservation laws which govern these complex processes is currently a controversial subject in the multiphase flow literature. No procedure is universally accepted and thus several different approaches have been employed. All current developments utilize a continuum approach which describe the field equations assuming the coexistence of the phases at every point in the flow field. It is in the derivation of these laws and in their final form where the controversy lies.

One approach to developing the two-phase flow equations involves bypassing the discrete nature of the separate phases through the use of averaging methods [of time, volume or mass; see, for example, Drew & Segel (1971) and Ishii (1975)]. In this case, the conservation equations are derived for averaged flow variables. Specific to reactive flow modeling is the work of Gough & Zwarts (1979) in which area averaging is used.

Another approach to the derivation of the field equations utilizes continuum mixture theory. In this case, conservation laws are determined for each phase which also account for the exchange of mass, momentum and energy between phases (i.e. drag etc.). In addition, conservation of mass, momentum and energy is required for the overall mixture [see Truesdell (1984) for details] and this imposes constraints on the interactions between phases. Typical problem formulations utilizing these types of conservation equations can be found in the text by Wallis (1969). Previous work using this approach which is relevant to DDT modeling includes the works of Krier and coworkers (Beckstead *et al.* 1977; Krier & Gokhale 1978; Butler *et al.* 1982), Kuo & Summerfield (1974) and Kooker (1981).

†This view of DDT is especially appropriate for solid explosives and has been described in the models of Macek (1959), Tarver *et al.* (1976) and Forest & Mader (1978). They treat the problem as one in which the gas generated due to combustion acts strictly as a "driving piston" on the material and does not permeate into the explosive. In this case, the onset of detonation occurs far in front of the flame front and is due to the coalescence of the pressure disturbances which result from the rapid gas generation behind the flame front.

In considering a complete treatment of reactive two-phase flow (total nonequilibrium), a closure problem exists. This problem results from including the volume fraction of a phase as an independent kinematic variable and can be seen by comparing the set of unknowns to the set of known relationships. For simplicity, we can consider two phases and one-dimensional flow. For each phase there are 5 quantities to be determined during flame spread, i.e. pressure, temperature, density, velocity and volume fraction; a total of 10 unknowns. The conservative laws (three for each phase), the state relation (one for each phase) and the volume constraint (sum of the volume fractions of all phases must be one) only result in 9 equations, and hence, the problem is underdetermined.

Previous studies of reactive multiphase flow have used several different approaches toward achieving closure. Some models consider the solid phase to be incompressible (e.g. Gough & Zwarts 1979). This constraint is incompatible with a solid equation of state since an infinite sound speed is implied. Bed compaction due to compressibility of the granular material as well as detonation cannot be meaningfully addressed with this approximation and thus this type of modeling can only be representative of reactive, two-phase flow with low-pressure gas generation (low pressure is to imply pressure regimes in which there is little compression and distortion of the solid grains).

Another type of constraint used in classical two-phase flow theory assumes pressure equilibrium between phases (e.g. Wallis 1969). This constraint produces a coupling of the sound speeds of the phases. This assumption is not acceptable, especially when it is recognized that to describe bed compaction during the transition to detonation, pressure nonequilibrium effects must be included. Previous work has also shown that the resulting conservation equations are ill-conditioned, implying that the solutions to the initial-value problem can be unstable. In particular, characteristics associated with the partial differential equations have been shown to be imaginary and thus wave motion is nonphysical. Previous work has suggested that elimination of the pressure equilibrium assumption removes these mathematical difficulties; see, for example, Stuhmiller (1977).

Another method of closure has been used by Krier and coworkers (Beckstead *et al.* 1977; Krier & Gokhale 1978; Butler *et al.* 1982) in which the pressures of the phases are not equal, but the pressure in the solid phase was defined in terms of the configuration changes of the granular material. This model is analogous to the p-α model† for porous materials proposed by Herrmann (1969), whereby bed compaction instanteously adjusts to produce local pressure equilibrium. This approach cannot describe rate-dependent compaction effects that are known to occur during the dynamic loading of granular materials (Butcher *et al.* 1974).

It is clear from these various approaches that model closure centers on the issue of describing the compressibility of each phase and the compaction of the granular bed. Recently, Nunziato & Walsh (1980), Passman (1977) and Passman *et al.* (1984) proposed a multiphase mixture theory which accounts for these effects using an additional conservation equation for the volume fraction of the solid. This equation is analogous to the pore collapse model developed by Carroll & Holt (1972) which is driven by pressure differences between the solid and gas phases and by the internal frictional effects of the granular bed. In this study, we shall adopt a similar approach to the problem of two-phase reactive flow and propose an evolutionary equation for the volume fraction consistent with thermodynamics. This equation is a simplified form of the Carroll & Holt model and the Passman, Nunziato & Walsh theory in that the inertial effects associated with bed compaction are assumed to be negligible. This approach results in a two-phase mixture theory similar to those discussed by Drumheller (1978) and Bowen (1984).

The two-phase reactive flow model proposed here is developed in the context of the continuum theory of multiphase mixtures. We then apply the theory to the problem of DDT in a column of pressed HMX grains. Specific constitutive models for the solid and gas phases are established using Hugoniot, thermo-physical and Chapman–Jouguet (CJ) detonation data. Additional constitutive equations are proposed for the interaction

†The α in this expression is the distention ratio, defined as the reciprocal of the solid volume fraction.

between phases which are consistent with thermodynamics. In this work, we employ a pressure-dependent burn law to describe the mass exchange, an experimentally-determined permeability for the drag coefficient in the momentum exchange and Gel'Perin & Ainstein's (1971) correlation for the heat-transfer coefficient in the energy exchange. The field equations are then solved numerically assuming an initial temperature and pressure in the gas phase corresponding to ignition and subsequent convective burning. The results, obtained for 70% dense HMX with an average surface-mean diameter of 100 μm, show that the transition occurs over a fairly short distance consistent with the experimental observations. We also report results on the effects of varying grain size and initial porosity and demonstrate a variety of dynamic compaction behavior by varying the compaction viscosity of the granular bed.

2. ONE-DIMENSIONAL THEORY FOR REACTIVE TWO-PHASE MIXTURES

2.1. Basic definitions

In this study, we will consider the behavior of a reacting, two-phase mixture of solid grains and a gas. The analysis, for simplicity, will be presented in a one-dimensional setting; although the extension to multidimensions is straightforward. Also, it should be noted that all variables will be subscripted with "a" to indicate that it is assigned to constituent a, either solid (S) or gas (G).†

At the outset, we assume that each constituent may occupy any given point x on the real line R at any time t and we assign to each phase a phase density $\gamma_a(x, t)$ and a volume fraction $\alpha_a(x, t)$. The phase density of a constituent is the mass per unit volume that it occupies, while the volume fraction of phase a represents the proportion of the total volume occupied by the constituent. The partial density ρ_a of phase a is determined by

$$\rho_a \equiv \alpha_a \gamma_a \tag{1}$$

and the mixture density ρ is the sum of partial densities,

$$\rho \equiv \sum \rho_a. \tag{2}$$

Since the solid particles and the gas are assumed to occupy all the volume available, the mixture is said to be saturated and

$$\sum \alpha_a = 1. \tag{3}$$

Each phase is also assigned a particle velocity $v_a(x, t)$ and the velocity of the mixture is the mass-weighted average of the constituent velocities:

$$v \equiv \sum \frac{\rho_a v_a}{\rho}. \tag{4}$$

In considering multiphase mixtures, it is convenient to define the material (or substantial) time derivative following the motion of a particular phase. If Γ_a is a quantity given in terms of the spatial position x and time t, the material time derivative of Γ_a can be computed using the chain rule:

$$\Gamma_a' = \frac{\partial \Gamma_a}{\partial t} + v_a \frac{\partial \Gamma_a}{\partial x}. \tag{5}$$

Similarly, the material time derivative of a quantity $\Gamma(x, t)$ following the motion of the mixture is

$$\dot{\Gamma} = \frac{\partial \Gamma}{\partial t} + v \frac{\partial \Gamma}{\partial x}. \tag{6}$$

†Throughout this work, we will use the terms "phase" and "constituent" interchangeably.

2.2. Conservation equations and entropy inequality

In this section, we consider the general forms of the conservation equations for each of the constituents and for the mixture. In specifying these equations, we make two important assumptions:

(i) each phase behaves as if it were a single material except when it is interacting and hence exchanging mass, momentum and energy with the other phase;

and

(ii) the conservation equations for the mixture are also the same as those for a single material and follow from summing the conservation equations for individual constituents over all constituents.

The first assumption implies that we can write for each phase the usual form of the conservation equations and account for the exchange of mass, momentum and energy by adding a supply term to each equation. Therefore, we have for each phase [see, for example, Truesdell (1984)]:

$$\rho_a' = -\rho_a \frac{\partial v_a}{\partial x} + c_a^+, \tag{7}$$

$$\rho_a v_a' = -\frac{\partial \pi_a}{\partial x} + \rho_a b_a + m_a^+ - c_a^+ v_a \tag{8}$$

and

$$\rho_a e_a' = -\pi_a \frac{\partial v_a}{\partial x} - \frac{\partial q_a}{\partial x} + \rho_a r_a + e_a^+ - m_a^+ v_a - c_a^+ (e_a - \tfrac{1}{2} v_a^2). \tag{9}$$

Equation [7] is a statement of conservation of mass and expresses the fact that the time rate of change of the partial density of the phase is related to the density change due to dilatation and the mass exchanged between phases due to chemical reactions, c_a^+. Equation [8] is a statement of conservation of linear momentum (Newton's second law). The rate of change of momentum of phase a is related to the gradient of the pressure π_a, the external body forces b_a (e.g. gravitational forces), the momentum transferred m_a^+ from one phase to another (i.e. drag) and the momentum associated with the appearance (or disappearance) of phase a. The remaining conservation law is a statement of the first law of thermodynamics as applied to each phase. The specific internal energy for each phase is represented by e_a. The material derivative of the internal energy is balanced by the work done by the pressure, conduction heat transfer q_a, external heat sources r_a (i.e. radiation), the exchange of energy between phases e_a^+, the energy associated with momentum transfer and the energy associated with appearance (or disappearance) of phase a.

Our second assumption asserts that if we sum the conservation equations over all constituents, then we should recover the usual conservation equations for a single substance. Indeed, carrying out this rather tedious calculation, we obtain the mixture equations

$$\dot{\rho} = -\rho \frac{\partial v}{\partial x}, \tag{10}$$

$$\rho \dot{v} = -\frac{\partial P}{\partial x} + \rho b \tag{11}$$

and

$$\rho \dot{e} = -P \frac{\partial v}{\partial x} - \frac{\partial q}{\partial x} + \rho r, \tag{12}$$

where

$$P + \rho v^2 = \sum (\pi_a + \rho_a v_a^2), \tag{13}$$

$$\rho b = \sum \rho_a b_a, \tag{14}$$

$$\rho\,(e + \tfrac{1}{2}v^2) = \sum \rho_a (e_a + \tfrac{1}{2}v_a^2), \tag{15}$$

$$q + Pv + \rho\,(e + \tfrac{1}{2}v^2)v = \sum [q_a + \pi_a v_a + \rho_a (e_a + \tfrac{1}{2}v_a^2)v_a] \tag{16}$$

and

$$\rho(r + bv) = \sum \rho_a (r_a + b_a v_a). \tag{17}$$

Expressions [13]–[17], along with [2]–[4], are often referred to as the *summing rules* for the mixture. Note that these definitions are consistent with the classical kinetic theory of gases. It should also be noted that the definition for the total pressure P includes inertial terms.

In writing [10]–[12] for the mixture, we have also required that the interactions c_a^+, m_a^+, e_a^+ satisfy the summing rules:

$$\sum c_a^+ = 0, \quad \sum m_a^+ = 0, \quad \sum e_a^+ = 0. \tag{18}$$

These summing rules impose important constraints on the processes possible in a two-phase mixture. For example, the first sum in [18] asserts that any mass loss of the grains due to combustion must be accounted for in the mass of the gas.

An important part of our study deals with the thermodynamics of the two-phase reactive flow. For each constituent of the flow we will assign an entropy, η_a, and an absolute temperature, T_a. Following the work of Truesdell (1984), the second law of thermodynamics can be stated as the entropy inequality

$$\sum \left[\rho_a \eta_a' + c_a^+ n_a + \frac{\partial}{\partial x}\left(\frac{1}{T_a} q_a\right) - \frac{\rho_a r_a}{T_a} \right] \geqslant 0. \tag{19}$$

Rather than working with the entropy, it is more convenient to introduce the Helmholtz free energy, ψ_a, given by

$$\psi_a = e_a - T_a \eta_a. \tag{20}$$

With this change of variable and substitution of the energy equation [9], the entropy inequality can be rewritten as

$$\sum \frac{1}{T_a}\left[-\rho_a(\eta_a T_a' + \psi_a') - \pi_a \frac{\partial v_a}{\partial x} - \frac{1}{T_a} q_a \frac{\partial T_a}{\partial x} - m_a^+ v_a + e_a^+ - (\psi_a - \tfrac{1}{2}v_a^2)c_a^+ \right] \geqslant 0. \tag{21}$$

This inequality imposes restrictions on the mixture's response. In the next section we will use [21] to obtain certain restrictions on the forms of the constitutive equations.

2.3. Thermodynamics of two-phase mixtures

In order to develop an understanding of the thermodynamically admissible processes in reactive flows involving granular materials, we need to consider the constitutive equations which describe the mixture's response. Here we propose such equations utilizing the principle of phase separation (Drew & Segel 1971; Passman *et al.* 1984). This principle expresses the idea that in a mixture of discrete phases, the free energy ψ_a, the pressure π_a, the entropy η_a and the heat flux q_a of a given constituent a depend only on the properties and the thermodynamic state of that constituent. On the other hand, the interactions, i.e. the mass, momentum and energy exchange, c_a^+, m_a^+, e_a^+, between the two phases depend on the properties and the thermodynamic states of both constituents. These statements can be expressed mathematically by writing constitutive equations of the form:

$$\begin{aligned} &\psi_a = \psi_a(S_a), \quad \pi_a = \pi_a(S_a), \quad \eta_a = \eta_a(S_a), \quad q_a = q_a(S_a), \\ &c_a^+ = c_a^+(S_S, S_G), \quad m_a^+ = m_a^+(S_S, S_G), \quad e_a^+ = e_a^+(S_S, S_G), \end{aligned} \tag{22}$$

where the thermodynamic state of constituent a ($a = \mathrm{S}, \mathrm{G}$) is the ordered array

$$S_a = \left\{ \alpha_a, T_a, \gamma_a, v_a, \frac{\partial T_a}{\partial x} \right\}. \qquad [23]$$

The precise form of these constitutive equations in any given application must reflect physical observations and be consistent with the entropy inequality [21].

It is important to note that this constitutive assumption is not sufficient to provide closure; that is, if the response of the mixture does indeed depend on the eight fields γ_a, T_a, α_a, v_a ($a = \mathrm{S}, \mathrm{G}$), then the set of six conservation equations [7]–[9] is incomplete. As we pointed out previously, various solutions to this difficulty have been proposed in the literature. Here we write an additional evolutionary equation for the volume fraction of each constituent:

$$\alpha_a' = f_a(S_\mathrm{S}, S_\mathrm{G}), \quad (\alpha = \mathrm{S}, \mathrm{G}). \qquad [24]$$

These equations permit us to account for both the compressibility of the constituents and the compaction of the granular bed by recognizing the volume fraction as an independent, internal degree of freedom within the mixture analogous to the internal degrees of freedom that arise in real gases (e.g. Vincenti & Kruger 1965). In essence, [24] imply that the compaction of the bed is rate dependent and, upon quasistatic loading and unloading, the bed can exhibit hysteresis.

We are now in a position to evaluate the restrictions the second law imposes on [22] and [24]. Using the chain rule, the rate of change of free energy is given by

$$\psi_a' = \frac{\partial \psi_a}{\partial \alpha_a}\alpha_a' + \frac{\partial \psi_a}{\partial T_a}T_a' + \frac{\partial \psi_a}{\partial \gamma_a}\gamma_a' + \frac{\partial \psi_a}{\partial v_a}v_a' + \frac{\partial \psi_a}{\partial\left(\dfrac{\partial T_a}{\partial x}\right)}\left(\overline{\frac{\partial T_a}{\partial x}}\right)'.$$

This result and conservation of mass [7], permits the entropy inequality [21] to be expressed as

$$\sum \frac{1}{T_a}\Bigg[-\rho_a\left(\eta_a + \frac{\partial \psi_a}{\partial T_a}\right)T_a' - (\pi_a - \alpha_a p_a)\frac{\partial v_a}{\partial x} - (\beta_a - p_a)\alpha_a' - \rho_a \frac{\partial \psi_a}{\partial v_a}v_a' - \rho_a \frac{\partial \psi_a}{\partial\left(\dfrac{\partial T_a}{\partial x}\right)}\left(\frac{\partial T}{\partial x}\right)'$$

$$- \frac{1}{T_a}q_a\frac{\partial T_a}{\partial x} + e_a^+ - m_a^+ v_a - c_a^+\left(\psi_a + \frac{p_a}{\gamma_a} - \frac{1}{2}v_a^2\right)\Bigg] \geqslant 0, \qquad [25]$$

where we have defined

$$p_a = \gamma_a^2 \frac{\partial \psi_a}{\partial \gamma_a} \qquad [26]$$

and

$$\beta_a = \alpha_a \gamma_a \frac{\partial \psi_a}{\partial \alpha_a}, \qquad [27]$$

as the *phase pressure* and the *configuration pressure*, respectively, of constituent a. The phase pressure describes the compressibility of the individual phases as represented by a mean or bulk stress. The configuration pressure β_a is clearly a consequence of changes in the packing of the granular bed, and hence β_S must reflect the contact forces between the grains.

Now, we require the above inequality to be satisfied for every thermodynamic process possible in the two-phase mixture described by the constitutive equations [22] and [24]. It is possible to construct certain processes such that T_a', $\partial v_a/\partial x$, v_a' and $(\partial T/\partial x)'$ can take on arbitrarily large values of the proper sign so that the inequality can be violated. Thus, the coefficients of these terms must vanish and we conclude that the Helmholtz free energy

is a function only of the state variables γ_a, T_a, α_a:

$$\psi_a = \hat{\psi}_a(\alpha_a, T_a, \gamma_a); \tag{28}$$

and that

$$\pi_a = \alpha_a p_a, \tag{29}$$

$$\eta_a = -\frac{\partial \psi_a}{\partial T_a}, \tag{30}$$

$$\sum \frac{1}{T_a}\left[e_a^+ - m_a^+ v_a - c_a^+\left(\psi_a + \frac{p_a}{\gamma_a} - \frac{1}{2}v_a^2\right) - (\beta_a - p_a)\alpha_a' - \frac{1}{T_a} q_a \frac{\partial T_a}{\partial x}\right] \geqslant 0. \tag{31}$$

The results [29] and [30] are familar from the classical theory of mixtures; [29] expresses the fact that the partial pressure of any phase is determined by volume-fraction weighting the phase pressure and [30] is the usual form of the entropy relation. The inequality [31] asserts that the dissipation in the mixture results from the exchange of mass, momentum and energy between constituents, heat conduction within the constituents and a viscous effect associated with the internal adjustments in volume fractions.

Finally, we note for future use that as a result of [20] and the entropy relation [30], the free energy ψ_a determines the internal energy e_a through the relation

$$e_a = \psi_a - T_a \frac{\partial \psi_a}{\partial T_a}. \tag{32}$$

2.4. Dissipation models and the governing partial differential equations

The dissipation inequality [31] provides information useful in formulating specific constitutive equations for the exchange functions c_a^+, m_a^+, e_a^+, the evolution of the volume fractions α_a', and the heat flux q_a. To this end, we need to rewrite [31] utilizing the constraints [3] and [18]:

$$c_G^+ = -c_S^+, \tag{33}$$

$$m_G^+ = -m_S^+, \tag{34}$$

$$e_G^+ = -e_S^+ \tag{35}$$

and

$$\alpha_G' = -\alpha_S' + (v_S - v_G)\frac{\partial \alpha_S}{\partial x}. \tag{36}$$

Thus, expanding [31], it is not difficult to show that

$$\begin{aligned} &-\frac{1}{T_S^2} q_S \frac{\partial T_S}{\partial x} - \frac{1}{T_G^2} q_G \frac{\partial T_G}{\partial x} + \frac{1}{T_G}\left(\alpha_S' - \frac{c_S^+}{\gamma_S}\right)[(p_S - \beta_S) - (p_G - \beta_G)] \\ &\quad + \left(\frac{1}{T_S} - \frac{1}{T_G}\right)\left[e_S^+ - m_S^+ v_S + (p_S - \beta_S)\left(\alpha_S' - \frac{c_S^+}{\gamma_S}\right) - c_S^+(e_S - \tfrac{1}{2}v_S^2)\right] \\ &\quad + \frac{1}{T_G}(v_S - v_G)\left[\frac{c_S^+}{2}(v_S + v_G) + (p_G - \beta_G)\frac{\partial \alpha_S}{\partial x} - m_S^+\right] \\ &\quad - \frac{c_S^+}{T_G \gamma_S}\left[\gamma_S(\psi_S - \psi_G) - \gamma_S(T_G - T_S)\eta_S + \left(\frac{T_G}{T_G}\beta_S - \beta_G\right) + p_G\left(\frac{\gamma_S}{\gamma_G} - 1\right)\right] \geqslant 0. \end{aligned} \tag{37}$$

In writing the inequality in this form, we have deliberately collected together terms involving temperature gradients, temperature differences, the difference between the

change in solid volume fraction and the volume lost by the solid grains due to combustion, velocity differences and the reaction rate—choices that are guided by physical intuition and/or experimental observations. In this form, [37] suggests specific constitutive equations for q_a, α_a', c_a^+, m_a^+ and e_a^+ which have clear physical interpretations. Specifically, we note that a sufficient, but *not* necessary, condition for satisfying [37] is to require each term of the inequality to be nonnegative. Then there exist nonnegative functions, k_a, h, μ_c, δ, ϵ which depend upon the thermodynamic state S_a of each phase, such that

$$q_a = -k_a \frac{\partial T_a}{\partial x}, \tag{38}$$

$$e_S^+ - m_S^+ v_S + (p_S - \beta_S)\left(\alpha_S' - \frac{c_S^+}{\gamma_S}\right) - c_S^+ (e_S - \tfrac{1}{2} v_S^2) = h(T_G - T_S), \tag{39}$$

$$\alpha_G \alpha_S [(p_S - \beta_S) - (p_G - \beta_G)] = \mu_c \left(\alpha_S' - \frac{c_S^+}{\gamma_S}\right), \tag{40}$$

$$\frac{c_S^+}{2}(v_S + v_G) + (p_G - \beta_G)\frac{\partial \alpha_S}{\partial x} - m_S^+ = \partial(v_S - v_G) \tag{41}$$

and

$$c_S^+ = -\epsilon \left\{ \frac{\gamma_S \gamma_G}{(\gamma_G - \gamma_S)} \left[(\psi_S - \psi_G) - (T_G - T_S)\eta_S + \left(\frac{T_G}{T_S}\beta_S - \beta_G\right)\frac{1}{\gamma_S} \right] + p_G \right\}. \tag{42}$$

These results can be rearranged to give

$$c_S^+ = -\epsilon(\theta + p_G), \tag{43}$$

$$m_S^+ = (p_G - \beta_G)\frac{\partial \alpha_S}{\partial x} - D + c_S^+ v_S, \tag{44}$$

$$e_S^+ = \left[(p_G - \beta_G)\frac{\partial \alpha_S}{\partial x} - D \right] v_s - (p_S - \beta_S)\left(\alpha_S' - \frac{c_S^+}{\gamma_S}\right) + c_S^+ (e_S + \tfrac{1}{2} v_S^2) + H, \tag{45}$$

$$\alpha_S' = \frac{\alpha_S \alpha_G}{\mu_c}[(p_S - \beta_S) - (p_G - \beta_G)] + \frac{c_S^+}{\gamma_S} \tag{46}$$

and

$$q_a = -k_a \frac{\partial T_a}{\partial x}, \tag{47}$$

where

$$\theta = \frac{\gamma_S \gamma_G}{(\gamma_G - \gamma_S)} \left[(\psi_S - \psi_G) - (T_G - T_S)\eta_S + \left(\frac{T_G}{T_S}\beta_S - \beta_G\right)\frac{1}{\gamma_S} \right], \tag{48}$$

$$D = (\delta + \tfrac{1}{2} c_S^+)(v_S - v_G) \tag{49}$$

and

$$H = h(T_G - T_S). \tag{50}$$

Each of these dissipation models reflects an important aspect of the combustion process in a granular bed. Equation [43] provides an expression for the kinetics of the chemical reaction associated with the burning of the grains. In particular, it represents the burn rate describing the mass exchange as linearly proportional to the gas pressure. Such a pressure dependence of the burn rate has been widely accepted in the combustion literature for some time and has generally been regarded as empirical (e.g. Williams 1965). Here we observe that the formula is consistent with thermodynamic restrictions. Also, we note that the coefficient θ in the burn law depends on the difference in free energies (ψ_S, ψ_G). Thus, consistent with classical thermochemistry, the burn rate model [43] in some sense reflects the amount of chemical energy available. The coefficient ϵ is physically related to the

surface-to-volume ratio for the grains and a characteristic time for the reaction. Hence ϵ will be referred to as simply the *kinetic shape factor*. The equation for the momentum exchange [44] includes the effect of the drag forces D acting on the particles due to the flowing gases and δ is referred to as the *drag coefficient*. It is important to remember that this coefficient depends on the geometry of the grains and is inversely proportional to the permeability of the granular bed. It is also clear from [44] and [49] that since c_S^+ is negative, the apparent drag force D on the burning grain is reduced and can conceivably change sign. The possibility of a negative drag has been suggested for ablating particles in high-speed gas flows (see Williams 1965; Crowe *et al.* 1963). The energy exchange given by [45] includes the work done by the drag forces, the work done in compacting the granular bed and the convective (Newton-type) energy transfer H that results from each phase having a different temperature. Here h is the *heat-transfer coefficient* and it too depends on the particle size. Equation [46] expresses the fact that changes in the volume fraction other than that due to combustion are related to pressure differences existing between phases and the configuration pressures. In this context, β_S and β_G are pressures which resist changes in the packing of the bed and hence compaction. Without loss in generality, we can ascribe this resistance to the contact forces acting on the solid and hence set $\beta_G \equiv 0$. It is useful to note in this case that the burn-rate coefficient θ reduces to

$$\theta = \frac{\gamma_S \gamma_G}{(\gamma_G - \gamma_S)}\left[(\psi_S - \psi_G) - (T_G - T_S)\eta_S + \frac{T_G}{T_S}\frac{\beta_S}{\gamma_S}\right] \qquad [51]$$

and it follows that the burn rate will increase with increasing resistance to bed compaction. The coefficient μ_c is interpreted as the *compaction viscosity* and if μ_c vanishes, then [46] implies that the pressure in the solid grains equals the pressure in the gas plus the pressure due to contact forces between the grains:

$$p_S = p_G + \beta_S. \qquad [52]$$

Finally, [47] expresses Fourier's law of heat conduction where k_a is the thermal conductivity of phase a.

Using the models [44]–[47] suggested by the dissipation inequality, along with [5] and the conservation equations [7]–[9], we obtain the partial differential equations governing DDT of granular explosives:

conservation of mass

$$\frac{\partial \rho_S}{\partial t} + \frac{\partial}{\partial x}(\rho_S v_S) = c_S^+ \qquad [53]$$

and

$$\frac{\partial \rho_G}{\partial t} + \frac{\partial}{\partial x}(\rho_G v_G) = -c_S^+; \qquad [54]$$

conservation of momentum

$$\rho_S\left[\frac{\partial v_S}{\partial t} + v_S\frac{\partial v_S}{\partial x}\right] = -\alpha_S\frac{\partial p_S}{\partial x} + (p_G - p_S)\frac{\partial \alpha_S}{\partial x} - (\delta + \tfrac{1}{2}c_S^+)(v_S - v_G) \qquad [55]$$

and

$$\rho_G\left[\frac{\partial v_G}{\partial t} + v_G\frac{\partial v_G}{\partial x}\right] = -\alpha_G\frac{\partial p_G}{\partial x} - (\delta - \tfrac{1}{2}c_S^+)(v_G - v_S); \qquad [56]$$

conservation of energy

$$\rho_S\left[\frac{\partial e_S}{\partial t} + v_S\frac{\partial e_S}{\partial x}\right] = -\alpha_S p_S\frac{\partial v_S}{\partial x} + \frac{\partial}{\partial x}\left(k_S\frac{\partial T_S}{\partial x}\right) + h(T_G - T_S) - (p_S - \beta_S)\left(\alpha_S' - \frac{c_S^+}{\gamma_S}\right) \qquad [57]$$

and

$$\rho_G\left[\frac{\partial e_G}{\partial t}+v_G\frac{\partial e_G}{\partial x}\right]=-\alpha_G p_G\frac{\partial v_G}{\partial x}+\frac{\partial}{\partial x}\left(k_G\frac{\partial T_G}{\partial x}\right)-h(T_G-T_S)$$
$$-\left[p_G\frac{\partial \alpha_S}{\partial x}-\delta(v_S-v_G)\right](v_S-v_G)+(p_S-\beta_S)\left(\alpha_S'-\frac{c_S^+}{\gamma_S}\right)+c_S^+(e_G-e_S); \quad [58]$$

compaction

$$\frac{\partial \alpha_S}{\partial t}+v_S\frac{\partial \alpha_S}{\partial x}=\frac{\alpha_S\alpha_G}{\mu_c}[p_S-(p_G+\beta_S)]+\frac{c_S^+}{\gamma_S} \quad [59]$$

and

$$\alpha_G=1-\alpha_S. \quad [60]$$

Here c_S^+ is given by [43] and p_a and e_a are determined by the Helmholtz free-energy function ψ_a through [26] and [32].

Upon inspection of these equations, it is evident that our theory also describes two other important effects governing flame spread and the subsequent formation of shock waves which lead to detonation. In the momentum equation for the solid [55], the term involving the pressure difference represents the forces associated with the motion of the grains when they are no longer in contact. In that instance, the pressure gradient term becomes small as $\alpha_S\to 0$. Secondly, the compressional energy associated with the pressure in the solid, p_S, influences the behavior of both the solid particles and the gas. Note also that both energy equations include convective energy transport.

3. EVALUATION OF THE CONSTITUTIVE EQUATIONS

Before solving the partial differential equations governing DDT given by [53]–[60], equations of state for the solid and gas-phases are specified and specific constitutive equations for the drag coefficient δ, the thermal conductivities k_a, the compaction viscosity μ_c, the heat-transfer coefficient h and the kinetic shape factor ϵ are determined. For the purpose of illustrating the main features of the theory and showing that it does describe the observed phenomena, we chose to consider a granular explosive which has been the subject of DDT studies in the past and whose physical properties are well-known. Hence we consider a column of HMX† grains pressed to 70% theoretical maximum density (TMD). The grains are assumed to be spherical with a 100 μm dia.

3.1. Equations of state

Important inputs to the multiphase model are the equation-of-state descriptions of the solid reactant and the gaseous combustion product. For the solid reactant, a thermoelastic description of the Helmholtz free energy (Sheffield *et al.* 1977) is used:

$$\psi_S(\gamma_S,T_S)=c_v^s\left\{(T_S-T_S^0)\left[1+\Gamma_S\gamma_S\left(\frac{1}{\gamma_S^0}-\frac{1}{\gamma_S}\right)\right]+T_s\ln\left(\frac{T_S^0}{T_S}\right)\right\}$$
$$+\frac{K_T}{\gamma_S^0N(N-1)}\left[\left(\frac{\gamma_S}{\gamma_S^0}\right)^{N-1}-(N-1)\left(1-\frac{\gamma_S^0}{\gamma_S}\right)-1\right]. \quad [61]$$

The constants in this description are obtained from Hugoniot and thermophysical data. The solid pressure and internal energy, p_S and e_S, are then obtained using the thermodynamic identities given in [26] and [32].

For the combustion product gas, an equation of state is employed that can describe the highly-expanded to the very-dense thermodynamic states. In this study, the

†HMX, $C_4H_8N_8O_8$, is a colorless polycrystalline explosive.

Jones–Wilkins–Lee (JWL) equation of state is used; see, for example, Kury *et al.* (1965) and Lee *et al.* (1968):

$$p_G = A\left(1 - \frac{\omega\gamma_G}{R_1\rho_S^0}\right)\exp\left(-\frac{R_1\rho_S^0}{\gamma_G}\right) + B\left(1 - \frac{\omega\gamma_G}{R_2\rho_S^0}\right)\exp\left(-\frac{R_2\rho_S^0}{\gamma_G}\right) + \omega\gamma_G e_G. \quad [62]$$

The state relationship is a five-parameter model (A, B, R_1, R_2, ω), whose constants are the best fits to experimental measurements and hydrodynamic calculations of explosively-driven cylindrical expansion experiments (Lee *et al.* 1968). This equation of state adequately reproduces the CJ detonation data (Stanton *et al.* 1981), when the constants are permitted to vary with the initial density of the reactant, ρ_S^0. Table 1 lists the equation-of-state and thermophysical data for HMX as taken from Gibbs and Popolato (1980) and Dobratz (1981). A thermodynamically consistent relationship for gas temperature is then determined from the thermodynamic relations [26] and [32]:

$$T_G = \frac{1}{c_v^G}\left[e_G + \Delta H_{det} - A\frac{\omega\gamma_G}{R_1\rho_S^0}\exp\left(-\frac{R_1\rho_S^0}{\gamma_G}\right) - B\frac{\omega\gamma_G}{R_2\rho_S^0}\exp\left(-\frac{R_2\rho_S^0}{\gamma_G}\right)\right], \quad [63]$$

where c_v^G is the gas specific heat and ΔH_{det} is the heat of detonation (estimated using thermochemical data).

3.2. Phase interactions

The remaining constitutive equations which are needed are the phase interactions describing the exchange of mass, momentum and energy between phases and the evolutionary equation for the solid volume fraction. Although the second law of thermodynamics has suggested a form of these constitutive equations, the coefficients of drag (δ) and heat transfer (h), the kinetic shape factor ϵ and the compaction viscosity μ_c have yet to be determined. Unfortunately, the only relationships currently available are empirically based and have not been experimentally tested under flow conditions corresponding to accelerated flame spread in a granular bed. Nevertheless, we shall adopt the existing correlations and assume that they hold in the appropriate flow regime.

First, we consider the burn law and the shape factor ϵ. As a result of thermodynamics, a burn rate is proposed of the form

$$c_S^+ = -\epsilon(\theta + p_G), \quad [64]$$

where θ is a function of the state of both the gas and solid. Although combustion occurs in the steps of solid decomposition, pyrolysis and gas-phase combustion, a simplified model, valid in the limit of fast chemistry, is used. Thus, the solid is directly converted

Table 1. Equation-of-state and thermophysical data

Variable [cgs units]	HMX ($\rho_S^0 = 1.33$ g/cm^3)
γ_S^0 [g/cm^3]	1.90
c_v^S [erg/g K]	1.5×10^7
K_T [dyn/cm^2]	1.35×10^{11}
$\Gamma_S\gamma_S$ [g/cm^3]	2.1
N	9.8
ΔH_{det} [erg/g]	7.9×10^{10}
A [dyn/cm^2]	2.4×10^{12}
B [dyn/cm^2]	5.0×10^9
R_1	4.2
R_2	1.0
ω	0.25
c_v^G [erg/g K]	2.4×10^7
k_G [erg/cm s K]	7.0×10^3
μ_G [gm/cm s]	5.0×10^{-4}
k_S [erg/cm s K]	4.0×10^4
μ_c [g/cm s]	1.0×10^4

to fully-reacted combustion product gas. In the present analysis, we will also assume that the gas pressure dependence of the burn law dominates the DDT and consequently approximate [64] with $p_G \gg \theta$. The resulting expression is of the standard form for pressure-dependent burn laws with a pressure exponent of unity. The combustion at the surface of a spherical particle suggests a shape factor, ϵ, consisting of three effects; the surface-to-volume ratio of the particle, the depletion of the particle, and a characteristic recession velocity w_S for individual grains. Thus, ϵ is given as

$$\epsilon = \frac{3\gamma_S(\alpha_S)^{2/3} w_S}{d_S(\alpha_S^0)^{1/3} p_G^{ref}}. \quad [65]$$

It is apparent that smaller particles and particles less densely packed burn more rapidly. These observations are consistent with experimental results on HMX (see Boggs *et al.* 1984). At a reference pressure of $p_G^{ref} = 10^9$ dyn/cm^2, the burn velocity of HMX, w_s, is approx. 10.0 cm/s.

Embodied in this simplified model is a description of the chemical reactions which actually occur during the combustion process; however, an ignition criterion is necessary. Although combustion begins at the grain surface, ignition may be achieved before the bulk temperature of the grain reaches the temperature which produces thermal decomposition of the grains. Thus, as a simplification, reaction is assumed when the volume-weighted temperature of the two-phase mixture reaches an "ignition" temperature, or

$$c_S^+ = 0 \quad \text{when} \quad (\alpha_S T_S + \alpha_G T_G) < T_{ign}. \quad [66]$$

The value of the constant T_{ign} was chosen to be 450 K which is the melt temperature of solid HMX. Detailed combustion models including local thermal and species structure of the gas and solid phases as well as models of the "hot spot" mechanisms are currently active areas of combustion physics research. Much has yet to be clarified before a more definitive ignition criteria is warranted in the modeling.

From the previous section, the drag force on the particles were shown to be of the form

$$D = (\delta + \tfrac{1}{2} c_S^+)(v_S - v_G). \quad [67]$$

Various models have been proposed in the literature for the drag coefficient δ. In this study we use a correlation obtained by Shepherd and Begeal (1983) as determined in an experimental study of shock-induced, high-speed gas flow in a porous bed shock tube. The interphasial drag was scaled to the Ergun (1952) relationship using the Darcy number as recommended by Dullien (1979):

$$\delta = \frac{\mu_G}{\kappa}\left(1 + \frac{\zeta_1 \mathrm{Re}}{\alpha_S}\right), \quad [68]$$

where μ_G is the gas viscosity and Re is the Reynolds number based on the initial grain diameter d_S:

$$\mathrm{Re} = \frac{\rho_G}{\mu_G}|v_G - v_S| d_S. \quad [69]$$

The κ is the experimental permeability deduced from the transient pressure drop measurements fit according to

$$\kappa = d_S^2 \alpha_G^{4.5}/\zeta_2; \quad [70]$$

ζ_1 and ζ_2 are data fit constants, respectively 0.01 and 33. The dependence of δ on the Reynolds number indicates that in high-speed flows, the gas flow is non-Darcy and that local inertial forces can be important since the drag coefficient δ increases with Reynolds number and solid volume fraction.

For the convective heat exchange between the particles and the gas,

$$H = h(T_G - T_S). \quad [71]$$

The heat-transfer coefficient h is given by a correlation by Gel'Perin & Ainstein (1971):

$$h = \frac{12\, k_G}{d_S^2} \alpha_G^{2/3} [1 + 0.2(\mathrm{Re})^{2/3}(\mathrm{Pr})^{1/3}], \quad [72]$$

where Pr is the gas Prandtl number defined by

$$\mathrm{Pr} = \frac{\mu_G c_v^G}{k_G}. \quad [73]$$

For the thermal conductivities of the phases, k_a, appropriate thermophysical data are used, as given in table 1. Additionally, a correction in the gas-phase conductivity has been included to treat thermal radiation from hot optically-thick combustion gases.

The evolutionary equation governing the change in the solid volume fraction α_S is new and has not been studied either experimentally or theoretically in the past. Consequently, we have no real basis on which to determine the compaction viscosity μ_c. As an approximation, μ_c is considered a constant whose magnitude is estimated using a simplified transport model similar to that posed in the kinetic theory of gases using the mean particle diameter, d_S, as the mean-free-path and the solid-phase sound speed, c_S:

$$\mu_c \sim \gamma_S c_S d_S. \quad [74]$$

The configurational stress, β_S, is estimated using experimental quasistatic compaction data inferred from the mechanical loading on a granular column. Figure 2 shows this stress at various solid volume fractions of HMX (Schwarz & Kopczewski 1982).

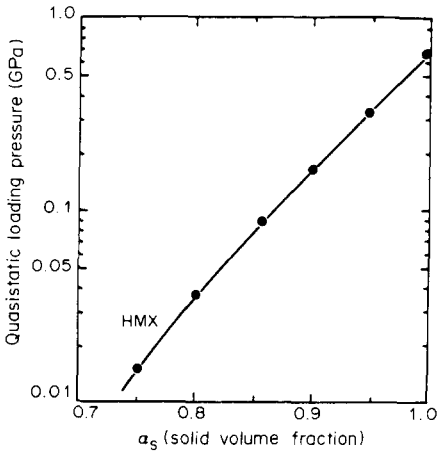

Figure 2. Quasistatic stress during pressing of an HMX granular column to various solid volume fractions.

4. NUMERICAL METHOD OF SOLUTION

4.1. Initial and boundary conditions

To evaluate the applicability of this multiphase flow model, the combustion and subsequent detonation of a column of granular explosive is considered. The effects of the lateral boundaries are neglected and thus the one-dimensional model outlined in section 2 is appropriate. In this view the column corresponds with an interval [O, L], of the real line R where L is the column length.

In formulating this problem, boundary conditions are prescribed at $x = 0$ and $x = L$. At the ignition end ($x = 0$), reflection boundary conditions are employed which yield vanishing gradients of the dependent variables: phase density, phase volume fraction, phase temperature and zero phase velocity. The zero velocity condition for the gas and solid also requires that the second derivative of mass flux be zero. Thus, at $x = 0$,

$$\frac{\partial \rho_a}{\partial x} = \frac{\partial \alpha_a}{\partial x} = \frac{\partial T_a}{\partial x} = 0, \quad t \geqslant 0, \quad [75]$$

and

$$\frac{\partial^2}{\partial x^2}(\rho_a v_a) = 0, \quad t \geqslant 0, \quad (a = \mathrm{S}, \mathrm{G}). \tag{76}$$

Note that by virtue of the results for the constitutive equations [26], [28], [32] and [47], [75] and [76] also imply

$$\frac{\partial p_a}{\partial x} = \frac{\partial e_a}{\partial x} = 0, \quad t \geqslant 0, \tag{77}$$

and

$$q_a = 0, \quad t \geqslant 0, \tag{78}$$

at $x = 0$, and hence there is no flux of heat at the ignition boundary. At the opposite end of the granular bed ($x = L$), zero gradients are imposed on all dependent variables. This permits material to flow out of that end of the column ($v_a \neq 0$) and thus there is no influence of the downstream conditions on the flow field.

For the present analysis, we will use the initial conditions to simulate an ignition condition which has resulted in a small burst of high-pressure (10^8 dyn/cm^2) hot combustion gases. Over a short distance L_1, $0 \leqslant x \leqslant L_1 \ll L$, a linear variation of gas pressure and temperature is assumed to initially exist in the bed:

$$p_{\mathrm{G}}(x, 0) = \begin{cases} (p_{\mathrm{G}})_1\left(1 - \dfrac{x}{L_1}\right), & 0 \leqslant x \leqslant L_1 \\ 0, & L_1 < x \leqslant L \end{cases} \tag{79}$$

and

$$T_{\mathrm{G}}(x, 0) = \begin{cases} (T_{\mathrm{G}})_1\left(1 - \dfrac{x}{L_1}\right), & 0 \leqslant x \leqslant L_1 \\ T_0, & L_1 < x \leqslant L, \end{cases} \tag{80}$$

where T_0 is the reference temperature of the bed (nominally 300 K). This suffices to initiate the combustion process in the bed provided the temperature $(T_{\mathrm{G}})_1$ resulting from the ignition source exceeds the ignition criterion for the solid grains.†

4.2. Numerical solution procedure

The numerical solution of the conservation equations [53]–[59] is obtained using a method-of-lines (MOL) approach. This method is easy to implement and takes full advantage of ordinary differential equation (ODE) solvers which have been extensively developed. Contrary to most finite-difference methods (e.g. Ames 1977) i.e. the Lax–Wendroff or McCormick methods, the space and time discretization of the partial differential equations (PDEs) are decoupled and analyzed independently. Temporal numerical stability is maintained by variable time-step control within the ODE solver.

The numerical formulation of the MOL follows closely the work of Hyman (1979), in which a general system of the conservative equations is considered:

$$\frac{\partial \mathbf{F}}{\partial t} = -\frac{\partial \mathbf{G}}{\partial x} + \mathbf{S}, \tag{81}$$

where $\mathbf{F}$ is the 7-dimensional vector whose elements are the dependent variables $(\rho_{\mathrm{S}}, \alpha_{\mathrm{S}}, v_{\mathrm{S}}, e_{\mathrm{S}}, \rho_{\mathrm{G}}, v_{\mathrm{G}}, e_{\mathrm{G}})$, $\mathbf{G}$ is the flux vector which can be a nonlinear function of $\mathbf{F}$, and $\mathbf{S}$ is the source vector. A discrete grid is then defined consisting of $N + 1$ points, denoted by an index i, with the left-hand boundary at $i = 1$ and the right-hand one at $i = N + 1$. At each node, the PDEs are evaluated:

$$\frac{\partial \mathbf{F}_i}{\partial t} = -\frac{\partial \mathbf{G}_i}{\partial x} + \mathbf{S}_i. \tag{82}$$

†In the present study, it is seen that as convective burning becomes established the initial ignition conditions are quickly modified due to the effects of gas permeation.

Space discretization of the flux vector $\mathbf{G}_i$ is then approximated using centered differences. To second order, $O(\Delta x)^2$, these are represented as

$$\frac{\partial \mathbf{G}_i}{\partial x} \simeq \frac{\mathbf{G}_{i+1} - \mathbf{G}_{i-1}}{2\Delta x} + O\left(\frac{1}{3}(\Delta x^2)\frac{\partial^3 \mathbf{G}_i}{\partial x^3}\right), \quad [83]$$

where $\Delta x = L/N$. It is to be noted that truncation of this approximation leads to errors of two classes: dispersion and dissipation. Some degree of dissipation is usually necessary to stabilize differencing methods and thus the choice of second-order spatial difference is made. An alternative approach would be to use higher-order differencing with the addition of increased artificial viscosity.

The boundary conditions at both ends of the column are incorporated in the differenced flux and the system of $N + 1$ ODEs are advanced with time, t. Thus, for $i = 1$,

$$\frac{d\mathbf{F}_1}{dt} = -\frac{\eta \mathbf{G}_1}{\Delta x} + \mathbf{S}_1, \quad [84]$$

where $\eta = 0$ if the flux is symmetric and $\eta = 1$ if the flux is asymmetric; and for $i = 2, \ldots, N$,

$$\frac{d\mathbf{F}_i}{dt} = \frac{(\mathbf{G}_{i-1} - \mathbf{G}_{i-1})}{2\Delta x} + \mathbf{S}_i. \quad [85]$$

The outflow boundary condition given at $i = N + 1$ is represented using

$$\frac{d\mathbf{F}_{N+1}}{dt} = \mathbf{S}_{N+1}. \quad [86]$$

The initial conditions for $\mathbf{F}_i$, $i = 1, 2, \ldots, N + 1$, are defined by the pressure and temperature variation in the gas due to the ignition source. Equations [84]–[86] consist of a system of $7(N + 1)$ ODEs which are solved using an implicit solver (DEBDF) developed by Shampine & Watts (1980). This integrator uses backward-difference formulas appropriate for the solution of stiff problems.

A frequent problem inherent in the numerical solution of hyperbolic conservation equations is the occurrence of nonphysical high-frequency waves or dispersive errors. The traditional method of reducing these effects is to introduce additional artificial dissipation in the equations (von Neuman & Richtmyer, 1950). In addition to the dissipation of truncation error, a minimal amount of additional artificial viscosity is used to provide sufficient local dissipation at shock fronts to satisfy Rankine–Hugoniot conditions. The form of artificial viscosity chosen in this study is that of Rusinov, in which a second-derivative dissipation term is included in all of the field equations:

$$\Psi_i = \nu \frac{\partial}{\partial x}\left(\lambda_c^a \frac{\partial \mathbf{F}_i}{\partial x}\right). \quad [87]$$

The artificial viscosity coefficient ν is chosen to be proportional to the grid spacing and λ_c^a is the maximum characteristic of the multiphase equations. As shown in the appendix, absolute characteristics are defined as

$$\lambda_c^a = |v_a| + c_a, \quad [88]$$

where c_a is the sound speed for phase a.

5. RESULTS

Using the aforementioned theory and model inputs, one-dimensional calculations are sought which describe flame spread in a 10 cm long column of HMX packed to a 70% initial density with uniform particles of a surface-mean diameter of 100 μm. The numerical grid was chosen to consist of 201 computational nodes distributed evenly throughout the column. (Several numerical experiments were performed with two- and four-fold increases in the number of computational nodes and only slight changes in the combustion wave characteristics were observed. This assured that adequate grid resolution was attained and that artificial viscosity effects were minimal.)

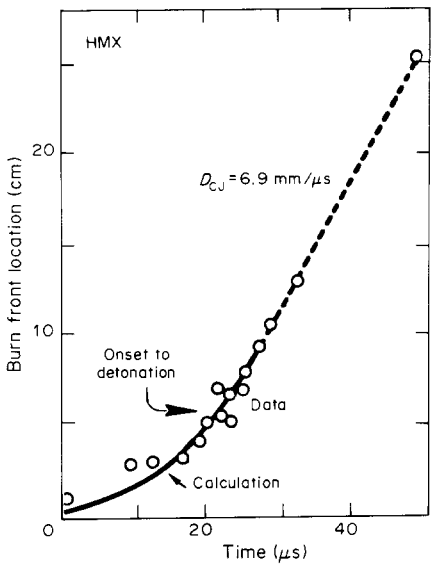

Figure 3. A comparison of the calculated and experimental distance–time burn front trajectory.

Displayed in figure 3 is a numerical–experimental comparison of the trajectory of the burn front with time. The experimental data was obtained by Price & Bernecker (1978), as determined by the triggering of ionization pins embedded in the granular bed. As seen in this comparison, burn duration, deflagration wave speed, detonation wave speed and the distance to detonation were reproduced well.

Details of the temporal and spatial variations of the solid and gas pressure, temperature, velocity and density are shown in figures 4–7 for the above baseline case. First, the evolution of solid and gas pressure is shown in figure 4. For the gas phase, early-time combustion behavior is dominated by the effects of gas permeation. Following ignition, a pressure gradient is produced that induces flow into the unreacted pores. Only a small rise in pressure (less than a few kilobar) is typical of this burning regime. As combustion continues, the gas generated in the primary flame zone exceeds that which can be permeated ahead of the combustion front and the rapid pressurization occurs. Since the combustion rate increases with gas pressure, continued pressurization occurs and a very large pressure gradient is eatablished. At this point, the inertial effects become important and the multiphase hydrodynamics form a compressive shock wave.

The solid pressure wave forms exhibit similar behavior. However, the similarity of the pressure wave forms is deceptive and by no means is pressure equilibrium to be implied. Details of the computations clearly indicate pressure differences of tens of kilobars, particularly near the combustion front. In these calculations, it is seen that the gas pressure leads that of the solid phase during the early phases of combustion and as the shock wave forms, the stress in the solid overtakes the leading gas pressure front, whereupon shock compression heating dominates the final stage of acceleration into detonation.

The solid and gas temperatures are shown in figure 5. During convective burning, the hot combustion gases are forced into the unreacted pores providing the mechanism of enhancing flame spread. As the combustion becomes accelerated, the gas within this zone is trapped and gas compression occurs as the bed becomes compacted. Quickly the gas temperatures rise to temperatures approaching 10,000 K. In experiments with heavily confined charges of crystalline explosives, streak camera observations of the burning columns indicate abrupt changes in radiance output from the high gas temperatures of the combustion flame front as compressive deflagration is initiated; see, for example, Baer *et al.* (1984). As the combustion gases expand, they cool to the temperatures predicted by equilibrium thermodynamics. The effect of compressional heating of the solid is seen during the later stage of burning into detonation.

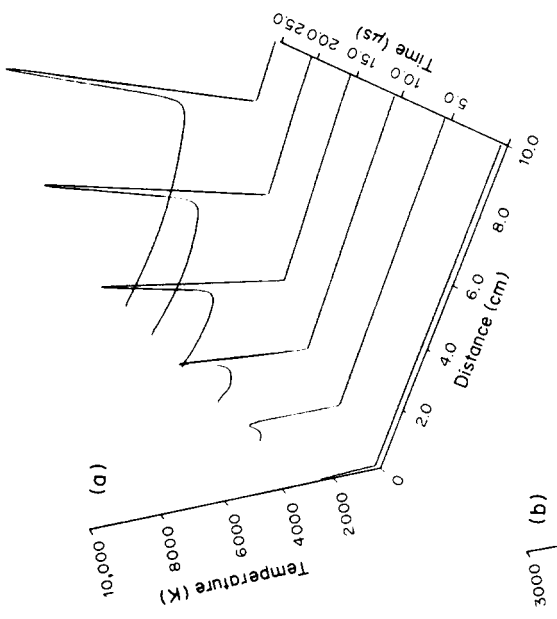

Figure 5. Temporal and spatial variations of (a) gas and (b) solid temperature during combustion of 70% dense HMX.

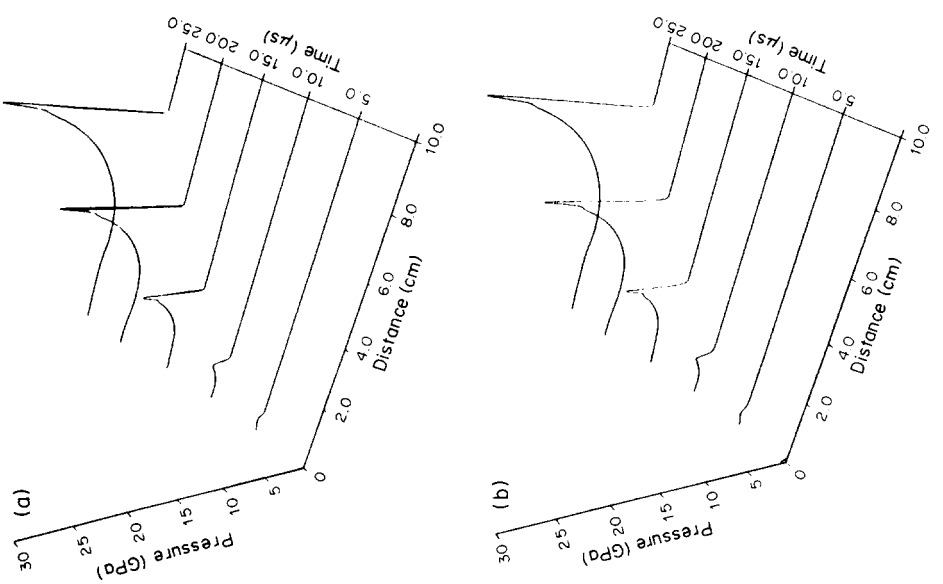

Figure 4. Temporal and spatial variations of (a) gas and (b) solid pressure during combustion of 70% dense HMX.

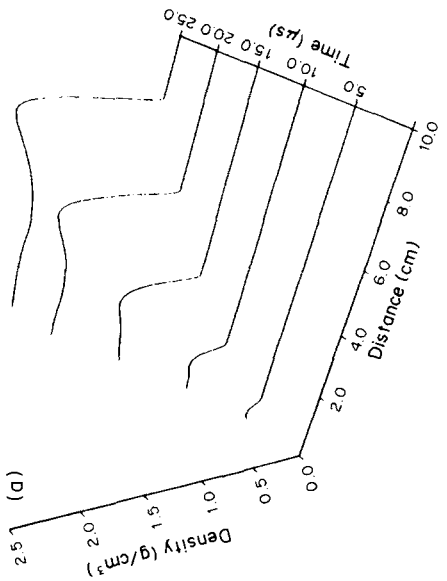

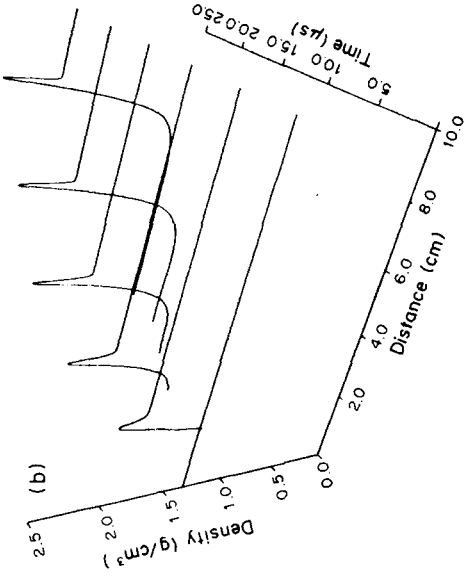

Figure 7. Temporal and spatial variations of (a) gas and (b) solid density during combustion of 70% dense HMX.

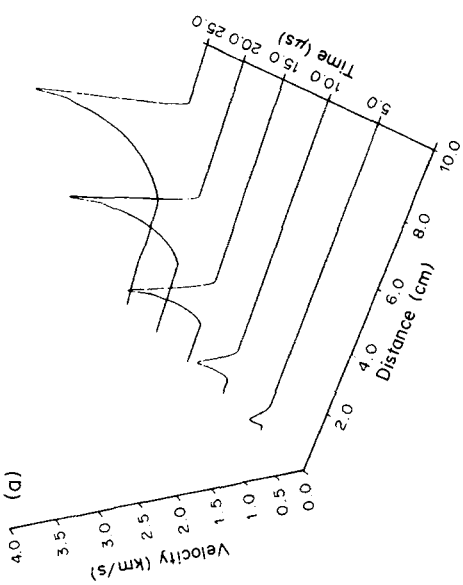

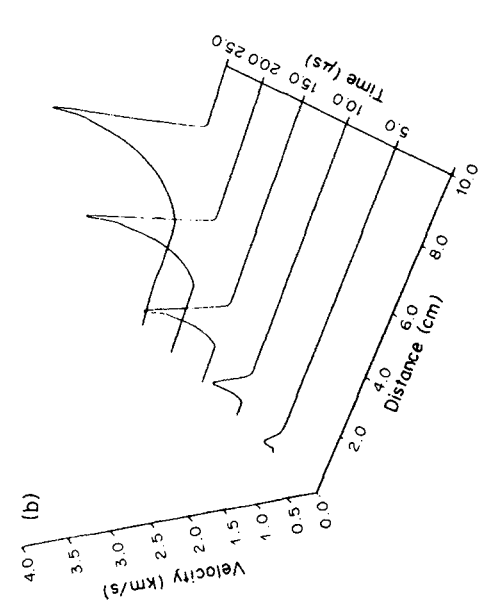

Figure 6. Temporal and spatial variations of (a) gas and (b) solid velocity during combustion of 70% dense HMX.

Shown in figure 6 are the gas- and solid-phase velocities. Similar wave forms are predicted for both phases which indicates strong influences of momentum exchange. It is the effect of interphase drag which causes mechanical load transfer from the gas to the solid phase, providing the mechanism for shock formation in the solid phase. The densities of the phases are shown in figure 7. Significant compressional effects for both phases are to be noted, particularly near the combustion front. As a characteristic of this gas–solid reactive flow, high-density combustion gases evolve as a result of the high confinement and high resistance of the gas flow into the bed. This result demonstrates the importance of using equations of state which can describe very dense thermodynamic states.

To display the development of compaction during combustion, the variations of the solid volume-fraction profiles are shown in figure 8. During convective burning significant compaction is seen ahead of the burn front. This wave grows in extent and amplitude to approx. 85% of the total void closure. However, with this greatly increased flow resistance, the gas permeation layer collapses and rapid pressurization accelerates the combustion and erodes away the compacted region faster than it can be formed. Finally, a steady compaction zone is achieved which propagates with the detonation wave.

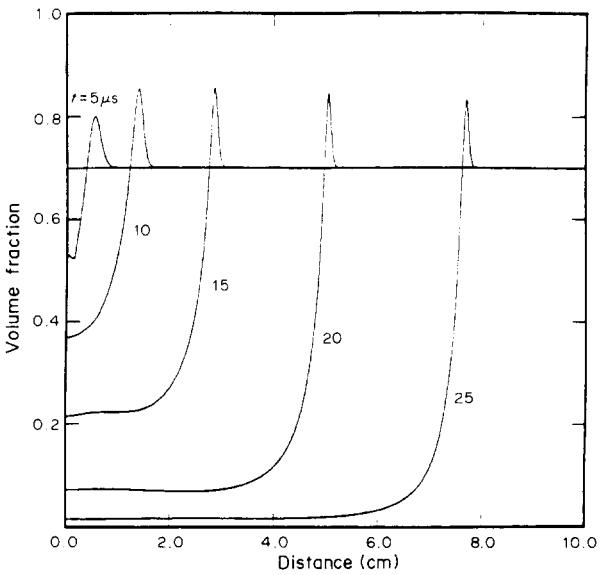

Figure 8. The evolution of the solid volume fraction during burning of HMX.

Since several phase interaction effects are dependent on the specific surface area of the granular material, calculations were performed varying the initial particle diameter, d_S, in a 70% dense HMX column. Figure 9 is a plot of the run distance to detonation at various particle diameters. The run distance to detonation was determined from the predicted ignition front trajectory as the predetonation length from the initiation of convective burning to the location of the onset of steady detonation. Shown in this figure are data by Price & Bernecker (1978) and Campbell (1980). Some offset to this data is seen which may be a result of the initial wave structure used to begin our calculations. Additionally, the initial particle size given in the experiments may not reflect a true particle size when packed in a dense column, since HMX is known to massively fracture during pressing. In spite of these uncertainties, the correct trends on the effect of particle size are predicted for $d_S > 20\,\mu$m and it is seen that the run length to detonation increases with increasing particle size (and subsequent reduction of specific surface area). For very fine HMX, detailed combustion models including pyrolysis and "hot spot" mechanisms may be necessary to attain better agreement between the calculations and experiments.

Figure 10a shows the variation of run length to detonation with the initial solid volume fraction. Similar to the findings of Griffiths & Groocock (1960), a minimum predetonation

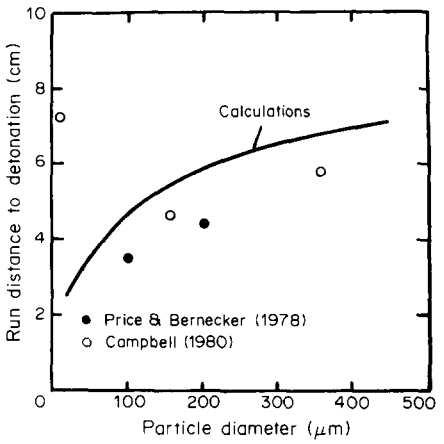

Figure 9. A comparison between calculated and experimental run length to detonation at various particles diameters.

length is predicted at an initial volume fraction of $\alpha_S^0 \sim 0.7$. As the porosity is increased, weakened drag forces allow more gas flow into the unreacted regions and thus slow the pressure buildup behind the flame front, which delays the onset to detonation. At the other extreme of low porosity, large amplitude compaction waves are formed which impede the convective burning process. In figure 10b the time to detonation (relative from the onset of convective burning) better demonstrates the effect of gas permeation. Interestingly, the minimum time to detonation occurs at an initial volume fraction of $\alpha_S^0 \sim 0.8$, which is the condition where compaction during combustion first achieves total void closure during combustion.

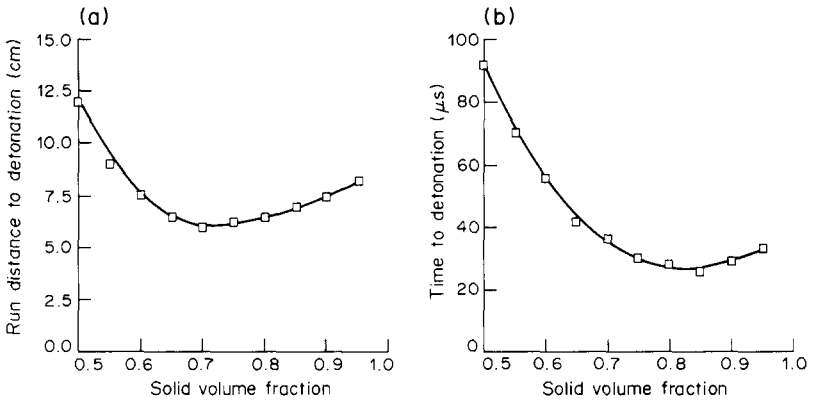

Figure 10. (a) The run length to detonation and (b) the time to detonation at various initial solid volume fractions of HMX with a surface-mean particle diameter of 200 μm.

In studying the effects of compaction during combustion, the combustion in a highly dense column of HMX ($\alpha_A^0 = 0.95$) was considered and the resulting wave profiles are shown in figures 11 and 12. The various wave features have been outlined on these plots. In the gas pressure figure, the gas permeation front extends from the maximum pressure during deflagration to the trailing edge of the compaction wave. As combustion grows into detonation, a pressure disturbance passing back into the reacted two-phase combustion region is seen as rapid combustion encounters a completely compacted plug. Very rapid pressurization is then seen to eventually produce a detonation wave structure.

In figure 12 the solid pressure plots show evidence of a compaction wave and a pressure disturbance of $\sim$4 kb propagating ahead of the gas permeation front. The onset of

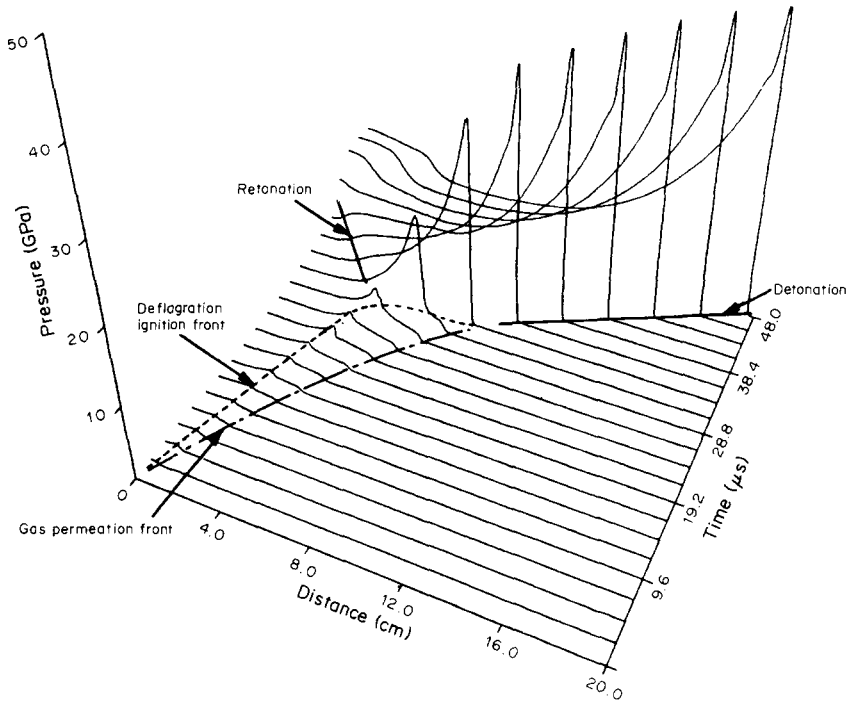

Figure 11. Gas pressure wave profiles during the combustion of 95% dense HMX.

detonation is seen as the point where the trailing and leading edges of the compaction wave coalesce. To better display these pressure waves, figure 13 is an overlay of solid and gas pressures at a time of 20 μs. Clearly, the pressure waves indicate nonequilibrium behavior. At this time, the extent of the zone of complete void closure is of length approx. 2 cm. Figure 14 shows the temporal variation of the solid volume fraction for this high-density case. It is evident that the formation and development of the compaction wave produces the delay in the onset to detonation.

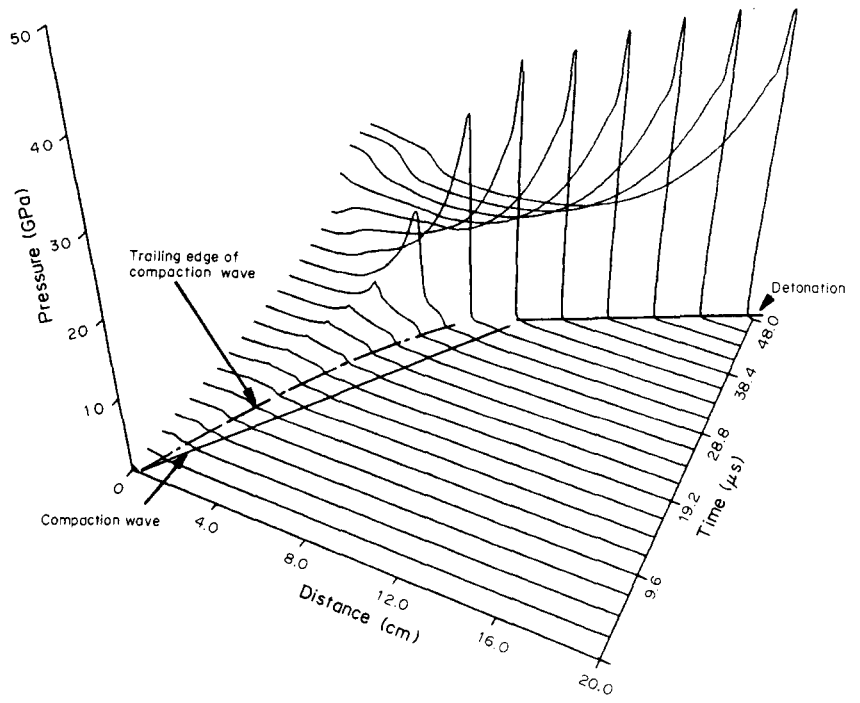

Figure 12. Solid pressure wave profiles during the combustion of 95% dense HMX.

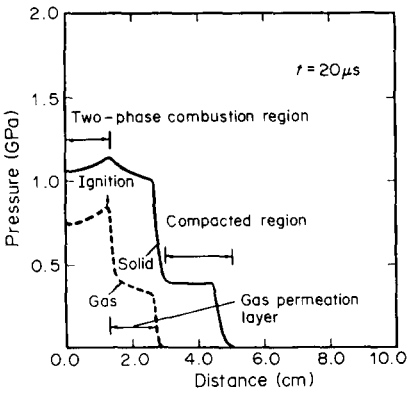

Figure 13. An overlay of gas and solid pressures at $t = 20\,\mu s$ showing the effects of compaction, gas permeation and two-phase combustion. Note the change in the pressure scale.

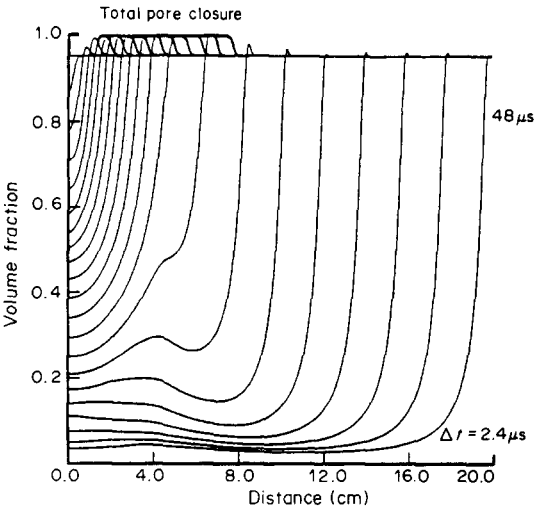

Figure 14. The evaluation of the solid volume fraction in 95% dense HMX showing the formation of a solid impermeable plug.

In a final series of calculations, the compaction wave behavior is studied by varying the compaction viscosity, μ_c. This parameter was varied from 10^3 to 10^6 g/cm s and the comparative pressure wave forms and the compaction wave structure are shown in figures 15–18 at 25 μs following ignition of a 70% dense HMX column. As the compaction viscosity is reduced, solid and gas pressures rapidly equilibrate, and a large amplitude compaction wave develops. However, at very high values of μ_c, pressures in both phases are greatly disparate and very little compaction occurs. From this result, it is evident that the rate of pressure equilibrium has a significant influence on the compaction behavior and more experimental guidance is needed to better assess a compaction model.

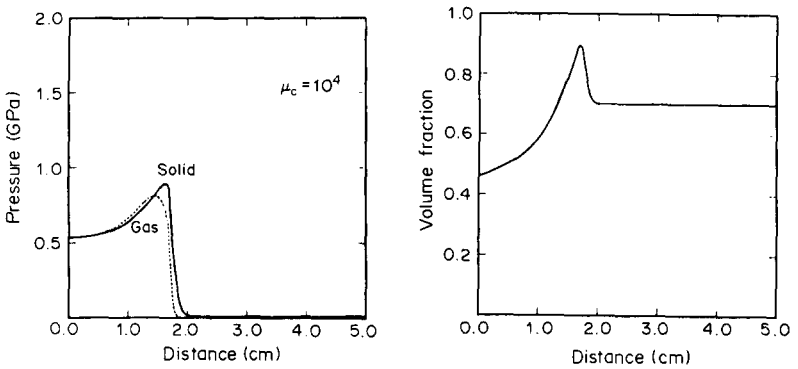

Figure 15. The gas–solid pressure wave profiles and the solid volume fraction at $t = 25\,\mu s$ during combustion of 70% dense HMX with $\mu_c = 10^4$ g/cm s.

6. SUMMARY

In this study, we have demonstrated that a reactive multiphase mixture model can adequately describe the complex combustion processes associated with convective burning, compressive deflagration and the growth to detonation in a granular explosive. The formulation of this thermodynamically-consistent model treats each phase as compressible and in complete thermodynamic nonequilibrium. Therefore, it is well-suited for description of the various thermal and mechanical processes leading to detonation. Although our studies have focused on the application of reactive multiphase flow, the framework of the

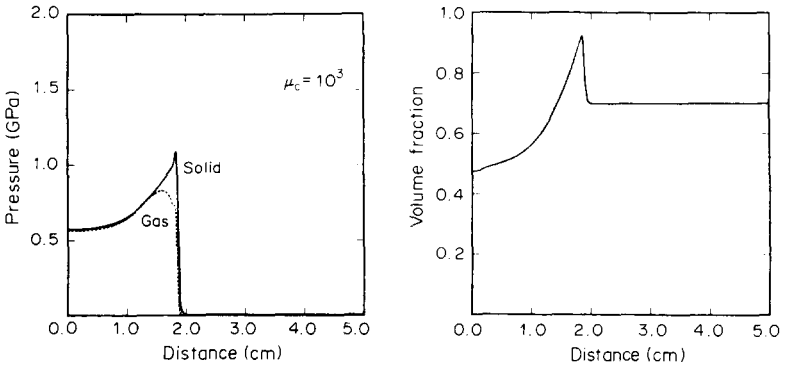

Figure 16. Baseline case at $t = 25\,\mu$s with $\mu_c = 10^3$ g/cm s. Pressures rapidly approach equilibrium and extensive compaction occurs.

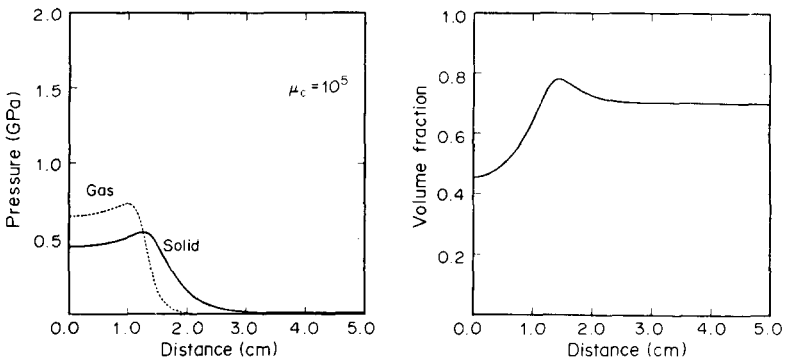

Figure 17. Baseline case at $t = 25\,\mu$s with $\mu_c = 10^5$ g/cm s.

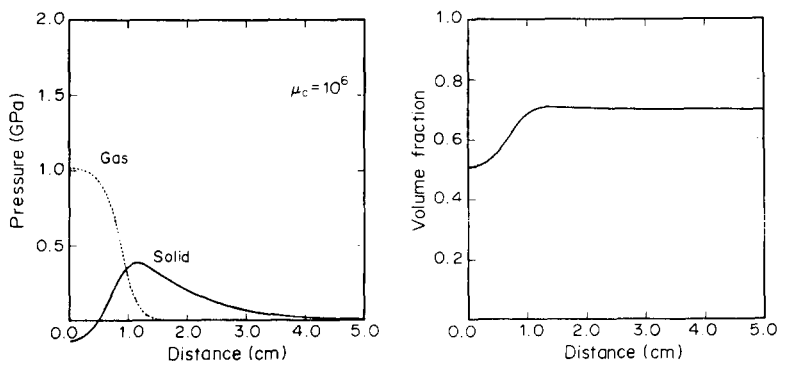

Figure 18. Baseline case at $t = 25\,\mu$s with $\mu_c = 10^6$ g/cm s. Pressures are disparate and little compaction occurs.

model may be applicable to other multiphase flows where nonequilibrium effects are suspected to be of major importance.

In this study of the flame spread in the explosive HMX, we have demonstrated adequate resolution of the combustion physics for situations where rapid gas pressurization is the dominant mode of producing DDT. The incorporation of detailed combustion models and micromechanical models describing various "hot spot" mechanisms will further expand the applications of the mixture model approach. Future work will be directed toward this implementation.

Acknowledgements—We gratefully acknowledge the many fruitful discussions with D. B. Hayes, J. E. Kennedy, P. Stanton, S. Passman (SNLA), H. Krier (University of Illinois) and E. K. Walsh (University of Florida). We also thank R. J. Gross (SNLA) for his assistance in programming the computer solutions and graphics display. Finally, we thank A. Treadway (SNLA) for his assistance in the characteristics analysis.

This work was performed at Sandia National Laboratories, supported by the U.S. Department of Energy, under Contract DE-AC04-76DP00789.

REFERENCES

AMES, W. F. 1977 *Numerical Methods for Partial Differential Equations*. Academic Press, New York.

ANDREEV, K. K. 1944 The problem of the mechanism of the transition from burning to detonation in explosives. *J. phys. Chem.* **17,** 533–537.

BAER, M. R. & NUNZIATO, J. W. 1982 A theory of deflagration-to-detonation transition in granular explosives. Report SAND82-0293, Sandia National Labs, Albuquerque, N.M.

BAER, M. R., IGEL, E. A., GROSS, R. J. & NUNZIATO, J. W. 1984 A study of deflagration-to-detonation transition (DDT) in the granular explosive, CP. Report SAND83-1929, Sandia National Labs, Albuquerque, N.M.

BECKSTEAD, M. W., PETERSON, N. L., PILCHER, D. T., HOPKINS, B. D. & KRIER, H. 1977 Convective combustion modeling applied to deflagration-to-detonation transition of HMX. *Combust. Flame* **30,** 231–241.

BERNECKER, R. R., SANDUSKY, H. W. & CLAIRMONT, A. R. 1981 Deflagration to detonation transition studies of porous explosive charges in plastic tubes. *Proc. 7th Symp. (Int.) on Detonation*, pp. 119–138.

BOGGS, T. L. 1984 The thermal behavior of cyclotrimethylenetrinitramine (RDX) and cyclotetramethylenetetranitramine (HMX). *Fundamentals of Solid-propellant Combustion* (Edited by KOU, K. & SUMMERFIELD, M.). *Prog. Astronaut. Aeronaut.* **90,** 121–175.

BOWEN, R. M. 1984 Diffusion models implied by the theory of mixtures. In *Rational Thermodynamics* (Edited by TRUESDELL, C.), pp. 237–263. Springer, New York.

BUTCHER, B. M., CARROLL, M. M. & HOLT, A. C. 1974 Shock-wave compaction of porous aluminum. *J. appl. Phys.* **45,** 3864–3875.

BUTLER, P. B., LEMBECK, M. F. & KRIER, H. 1982 Modeling of shock development and transition to detonation initiated by burning in porous propellant beds. *Combust. Flame* **46,** 75–93.

CAMPBELL, A. W. 1980 Deflagration-to-detonation transition in granular HMX. *Proc. 1980 JANNAF Propulsion System Hazards Subcommittee Mtg*, Los Alamos, N.M., pp. 105–130.

CARROLL, M. M. & HOLT, A. 1972 Static and dynamic pore-collapse for ductile porous materials. *J. appl. Phys.* **43,** 1626–1635.

COURANT, R. & HILBERT, D. 1962 *Methods of Mathematical Physics*, Vol. II. Interscience, New York.

CROWE, C. T., NICHOLLS, J. A. & MORRISON, R. B. 1963 Drag coefficients of inert and burning particles accelerating in gas streams. *Proc. 9th Symp. (Int.) on Combustion*, pp. 395–406.

DOBRATZ, B. M. 1981 LLNL explosives handbook: properties of chemical explosives and chemical simulants. Report UCRL-52997.

DREW, D. A. & SEGEL L. A. 1971 Averaged equations for two-phase flows. *Stud. appl. Math.* **1,** 205–231.

DRUMHELLER, D. S. 1978 The theoretical treatment of a porous solid using a mixture theory. *Int. J. Solids Struct.* **14,** 441–450.

DULLIEN, F. A. L. 1979 *Porous Media Fluid Transport and Pore Structure*. Academic Press, New York.

ERGUN, S. 1952 Fluid flow through packed columns. *Chem. Engng Prog.* **48,** 89–94.

FOREST, C. A. & MADER, C. L. 1978 Numerical modeling of the deflagration to detonation transition. *Proc. 17th Symp. (Int.) on Combustion*, pp. 35–41.

GEL'PERIN, N. I. & AINSTEIN, V. G. 1971 Heat transfer in fluidized beds. In *Fluidization.* Academic Press, New York.

GIBBS, T. R. & POPOLATO, A. 1980 *LASL Explosive Property Data.* Univ. of California Press, Berkeley, Calif.

GOUGH, P. S. & ZWARTS, F. J. 1979 Modeling heterogeneous two-phase reacting flow. *AIAA Jl* **17,** 17–25.

GRIFFITHS, N. & GROOCOCK, J. M. 1960 Burning to detonation of solid explosives. *J. chem. Soc., Lond.*, **814,** 4154–4162.

HERRMANN, W. 1969 Constitutive equation for the dynamic compaction of ductile porous materials. *J. appl. Phys.* **40,** 2490–2499.

HICKS, D. L. 1980 Well-posedness of the two-phase problem, Part 2: stability analyses and microstructural models. Report SAND80-1276, Sandia National Labs, Albuquerque, N.M.

HYMAN, J. M. 1979 A method of lines approach to the numerical solution of conservation laws. Report LA-VR 79-837, Los Alamos National Labs, Los Alamos, N.M.

ISHII, M. 1975 *Thermo-fluid Dynamic Theory of Two-phase Flow.* Eyrolles, Paris.

KOOKER, D. E. & ANDERSON, R. D. 1981 A mechanism for the burning rate of high density, porous energetic materials. *Proc. 7th Symp. (Int.) on Detonation*, pp. 198–215.

KRIER, H. & GOKHALE, S. S. 1978 Modeling of convective mode combustion through granulated propellant to predict detonation transition. *AIAA Jl* **16,** 177–183.

KUO, K. K. & SUMMERFIELD, M. 1974 High speed combustion of mobile granular solid propellants: wave structure and the equivalent Rankine–Hugoniot relation. *Proc. 15th Symp. (Int.) on Combustion*, pp. 515–527.

KURY, J. W., HORNIG, H. C., LEE, E. L., MCDONNEL, J. L., ORNELLAS, D. L., FINGER, M., STRANGE, F. M. & WILKINS, M. L. 1965 Metal acceleration by chemical explosives. *Proc. 4th Symp. (Int.) on Detonation*, pp. 3–10.

LEE, E., HORNIG, H. C. & KURY, J. W. 1968 Adiabatic expansion of high explosive detonation products. Report LNLL VCRL-50422.

MACEK, A. 1959 Transition from deflagration to detonation in cast explosives. *J. chem. Phys.* **31,** 162–167.

VON NEUMANN, J. & RICHTMYER, R. D. 1950 A method for the numerical calculations of hydrodynamic shocks. *J. appl. Phys.* **21,** 232–237.

NUNZIATO, J. W. 1984 Initiation and growth-to-detonation in reactive mixtures. In *Shock Waves in Condensed Matter—1983* (Edited by ASSAY, J. R., GRAHAM, R. A. & STRAUB, G. K.), pp. 581–588. Elsevier, New York.

NUNZIATO, J. W. & WALSH, E. K. 1977 On ideal multiphase mixtures with chemical reactions and diffusion. *Archs Rational Mech. Analysis* **73,** 285–311.

PASSMAN, S. 1977 Mixtures of granular materials. *Int. J. Engng Sci.* **15,** 117–129.

PASSMAN, S. L., NUNZIATO, J. W. & WALSH, E. K. 1984 A theory of multiphase mixtures. In *Rational Thermodynamics* (Edited by TRUESDELL, C.), pp. 286–325, McGraw–Hill, New York, 1984.

PRICE, D. & BERNECKER, R. R. 1978 Effect of wax on the deflagration to detonation transition of porous explosives. In *Behavior of Dense Media Under High Dynamic Pressure*, pp. 149–159. Commissariat a l'Energie Atomique, Paris.

SANDUSKY, H. W. 1983 Compressive ignition and burning in porous beds of energetic materials. *Proc. 1983 JANNAF Propulsion System Hazards Subcommittee Mtg*, Los Alamos, N.M., pp. 249–257.

SCHWARZ, A. C. & KOPCZEWSKI, M. R. 1982 Status report: development of a low-voltage, all-secondary detonator. Internal Memo RS2515/18/23, Sandia National Labs, Albuquerque, N.M.

SHAMPINE, L. F. & WATTS, H. A. 1980 DEPAC—design of a user oriented package of ODE solvers. Report SAND79-2374, Sandia National Labs, Albuquerque, N.M.

SHEFFIELD, S. A., MITCHELL, D. E. & HAYES, D. B. 1977 An equation of state and chemical kinetics for hexanitrostilbene (HNS) explosive. *Proc. 6th Symp. (Int.) on Detonation*, pp. 748–754.

SHEPHERD, J. & BEGEAL, D. 1983 Transient compressible flow in porous materials. Report SAND83-1788, Sandia National Labs, Albuquerque, N.M.

STANTON, P. L. 1982 Personal communication, Sandia National Labs, Albuquerque, N.M.

STANTON, P. L., IGEL, E. A., LEE, L. M., MOHLER, J. M. & WEST, G. T. 1981 Characterization of the DDT explosive, CP. *Proc. 7th Symp. (Int.) on Detonation*, pp. 865–876.

STUHMILLER, J. H. 1977 The influence of interfacial pressure forces on the character of two-phase flow model equations. *Int. J. Multiphase Flow* **3**, 551–560.

TARVER, C. M., GOODALE, T. C., SHAW, K. & COWPERTHWAITE, M. 1976 Deflagration to detonation transition studies for two cast primary explosives. *Proc. 6th Symp. (Int.) on Detonation*, pp. 231–249.

TRUESDELL, C. 1984 *Rational Thermodynamics*. McGraw-Hill, New York.

VAN TASSEL, W. F. & KRIER, H. 1975 Combustion and flame spreading phenomena in gas-permeable explosive materials. *Int. J. Heat Mass Transfer* **18**, 1377–1385.

VINCENTI, W. G. & KRUGER C. H. 1965 *Introduction to Physical Gas Dynamics*. Wiley, New York.

WALLIS, G. 1969 *One-dimensional Two-phase Flow*. McGraw-Hill, New York.

WILLIAMS, F. A. 1965 *Combustion Theory*. Addison-Wesley, Reading, Mass.

APPENDIX

Characteristics of Two-phase Mixture Equations

In this appendix, the characteristics (or eigenvalues) of the proposed multiphase field equations are determined, following Courant & Hilbert (1962), to demonstrate that these equations are stable in the sense of von Neuman [see, for example, Hicks (1980)]. Thus, wave motion described by these equations is physically and mathematically well-posed.

In this analysis, the following definitions are first provided:

$$m_a = \rho_a v_a, \quad E_a = \rho_a(e_a + \tfrac{1}{2}v_a^2), \quad (a = \mathrm{S}, \mathrm{G}).$$

The state vector, $\mathbf{F}$, is then defined as

$$\mathbf{F}^{\mathrm{T}} = \{\rho_{\mathrm{S}}, m_{\mathrm{S}}, E_{\mathrm{S}}, \gamma_{\mathrm{S}}, \rho_{\mathrm{G}}, m_{\mathrm{G}}, E_{\mathrm{G}}\}.$$

For a two-phase system, the density variables are related using the saturation constraint and by the definition

$$\gamma_{\mathrm{G}} = \frac{\gamma_{\mathrm{S}}\rho_{\mathrm{G}}}{(\gamma_{\mathrm{S}} - \rho_{\mathrm{S}})}.$$

Additionally, the Grüneisen coefficient for each phase, Γ_a, is defined as

$$\Gamma_a = \frac{1}{\gamma_a}\left(\frac{\partial p_a}{\partial e_a}\right);$$

and the frozen sound speed, c_a, is determined by

$$c_a^2 = \left(\frac{\partial p_a}{\partial \gamma_a}\right)_{e_a} + \frac{p_a\Gamma_a}{\gamma_a}.$$

The field equations given by [53]–[59] are recast into the state vector variables, excluding the diffusive conduction flux, and generalized into the form

$$\frac{\partial \mathbf{F}}{\partial t} + \mathbb{B}(\mathbf{F})\frac{\partial \mathbf{F}}{\partial x} = \mathbb{S}(\mathbf{F}),$$

where $\mathbb{B}(\mathbf{F})$ is a real 7×7 array.

The eigenvalues of the $\mathbb{B}(\mathbf{F})$ matrix are determined by

$$\det|\mathbb{B} - \lambda\mathbb{I}| = 0.$$

The structure of the matrix is

$$\left[\begin{array}{cccc|ccc} -\lambda & 1 & 0 & 0 & 0 & 0 & 0 \\ B_{21} & (B_{22}-\lambda) & B_{23} & B_{24} & 0 & 0 & 0 \\ B_{31} & B_{32} & (B_{33}-\lambda) & B_{34} & 0 & 0 & 0 \\ B_{41} & B_{42} & 0 & (B_{44}-\lambda) & 0 & 0 & 0 \\ \hline 0 & 0 & 0 & 0 & -\lambda & 1 & 0 \\ B_{61} & 0 & 0 & B_{64} & B_{65} & (B_{66}-\lambda) & B_{67} \\ B_{71} & 0 & 0 & B_{74} & B_{75} & B_{76} & (B_{77}-\lambda) \end{array}\right],$$

where:

$$B_{21}=\frac{(p_S-p_G)}{\gamma_S}-\frac{m_S^2}{\rho_S^2}-\frac{\Gamma_S}{\rho_S}\left(E_S-\frac{m_S^2}{\rho_S}\right);\quad B_{31}=\frac{m_S}{\rho_S}\left(B_{21}+\frac{m_S^2}{\rho_S^2}-\frac{E_S}{\rho_S}-\frac{p_S}{\gamma_S}\right);$$

$$B_{41}=-\frac{\gamma_S m_S}{\rho_S^2};\quad B_{61}=\frac{\gamma_G}{\gamma_S}\left(c_G^2-\frac{p_G\Gamma_G}{\gamma_G}\right);\quad B_{71}=\frac{m_G B_{61}}{\rho_G}+\frac{p_G}{\gamma_G}\left(\frac{m_S}{\rho_S}-\frac{m_G}{\rho_G}\right);$$

$$B_{22}=\frac{m_S}{\rho_S}(2-\Gamma_S);\quad B_{32}=\frac{E_S}{\rho_S}+\frac{p_S}{\gamma_S}-\frac{m_S^2\Gamma_S}{\rho_S^2};\quad B_{42}=\frac{\gamma_S}{\rho_S};\quad B_{23}=\Gamma_S;$$

$$B_{33}=\frac{m_S}{\rho_S}(1+\Gamma_S);\quad B_{24}=\frac{\rho_S}{\gamma_S}\left[c_S^2-\frac{p_S\Gamma_S}{\gamma_S}-\frac{(p_S-p_G)}{\gamma_S}\right];$$

$$B_{34}=\frac{m_S B_{24}}{\rho_S};\quad B_{44}=\frac{m_S}{\rho_S};\quad B_{64}=-\left(c_G^2-\frac{p_G\Gamma_G}{\gamma_G}\right)\frac{\rho_S\gamma_G}{\gamma_S^2};$$

$$B_{74}=-\frac{m_G B_{64}}{\gamma_G}-\left(\frac{m_S}{\rho_S}-\frac{m_G}{\rho_G}\right)\frac{p_S\rho_S}{\gamma_S^2};\quad B_{65}=c_G^2-\frac{p_G\Gamma_G}{\gamma_G}-\frac{m_G^2}{\rho_G^2}-\frac{\Gamma_G}{\rho_G}\left(E_G-\frac{m_G^2}{\rho_G}\right);$$

$$B_{75}=\frac{m_G}{\rho_G}\left(B_{65}+\frac{m_G^2}{\rho_G^2}-\frac{E_G}{\rho_G}-\frac{p_G}{\gamma_G}\right);\quad B_{66}=\frac{m_G}{\rho_G}(2-\Gamma_G);$$

$$B_{76}=\frac{E_G}{\rho_G}+\frac{p_G}{\gamma_G}-\frac{m_G^2\Gamma_G}{\rho_G^2};\quad \text{and}\quad B_{67}=\Gamma_G;\quad B_{77}=\frac{m_G}{\rho_G}(1+\Gamma_G).$$

Accordingly, the lower right 3×3 and the upper left 4×4 submatrices can be triangularized independently of the rest of the matrix. Therefore, the eigenvalues of the complete matrix are given by the products of the eigenvalues of the submatrices. After reducing the algebra, the determinate is factored as

$$(\lambda-v_S)^2(\lambda-v_S+c_S)(\lambda-v_S-c_S)(\lambda-v_G)(\lambda-v_G+c_G)(\lambda-v_G-c_G)=0,$$

which yields the following array of roots:

$$\lambda^{\mathrm{T}}=\{v_S, v_S, v_S\pm c_S, v_G, v_G\pm c_G\}.$$

All characteristics are seen to be real, as required for stability.

Interestingly, one sees that the characteristics depend *only on single-phase variables* and can be separated as those belonging to the solid phase λ_i^S $(i=1,\ldots,4)$, and those to the gas phase λ_i^G $(i=5,\ldots,7)$. In the limit, as one phase vanishes from the system, the set conforms to well-known single-phase eigenvalues.

The associated eigenvectors, l_j^i $(i,j=1,\ldots,7)$, can then be determined. The left eigenvectors are define, viz.

$$l_i^{\mathrm{T}}(\mathbb{B}-\lambda_i\mathbb{I})=\mathbf{0}$$

or

$$(\mathbb{B}^{\mathrm{T}} - \lambda_i \mathbb{I}) l_i = \mathbf{0},$$

and the system of equations is said to be hyperbolic if the eigenvectors are independent and the field equations can then be transformed into characteristic form:

$$l^{\mathrm{T}}\left(\frac{\partial \mathbf{F}}{\partial t} + \lambda \frac{\partial \mathbf{F}}{\partial x}\right) = l^{\mathrm{T}} \mathbb{S}(\mathbf{F}).$$

It is noted that if $\lambda_i^{\mathrm{S}} \neq \lambda_i^{\mathrm{G}}$ and $\lambda = \lambda_i^{\mathrm{S}}$, the solution to

$$\begin{pmatrix} -\lambda_i^{\mathrm{S}} & B_{65} & B_{75} \\ 1 & (B_{66} - \lambda_i^{\mathrm{S}}) & B_{76} \\ 0 & B_{67} & (B_{77} - \lambda_i^{\mathrm{S}}) \end{pmatrix} \begin{pmatrix} l_5^i \\ l_6^i \\ l_7^i \end{pmatrix} = 0$$

requires $l_j^i = 0$ $(j = 5, \ldots, 7)$. As such, the dependent variables on the l.h.s. of the solid-phase equations (in characteristic form) consist only of solid-phase variables. However, for $\lambda = \lambda_i^{\mathrm{G}}$, $l_j^i \neq 0$ and the compatibility equations represent total-phase equations. Since the v_{S} eigenvalue is repeated, the independence of the associated eigenvectors is checked by substituting $\lambda = v_{\mathrm{S}}$ and solving for the eigenvectors. These independent vectors are

$$l_1^{\mathrm{T}} = \left\{ -\left(e_{\mathrm{S}} + \frac{p_{\mathrm{S}}}{\gamma_{\mathrm{S}}} - \frac{v_{\mathrm{S}}^2}{2}\right), -v_{\mathrm{S}}, 1, 0, 0, 0, 0 \right\},$$

and

$$l_2^{\mathrm{T}} = \{0, 0, 0, 1, 0, 0, 0\}.$$